# Dalton Transactions

Accepted Manuscript






ROYAL SOCIETY OF CHEMISTRY

www.rsc.org/dalton

# Mechanism and Stability of Spectrally Pure Green Up-conversion Emission in $Yb^{3+}/Ho^{3+}$ Co-doped $Ba_5Gd_8Zn_4O_{21}$ Phosphor

Hao Suo[a], Chongfeng Guo[a*], Wenbin Wang[a], Ting Li[a], Changkuai Duan[b], Min Yin[b]

a. *National Key Laboratory of Photoelectric Technology and Functional Materials (Culture Base) in Shaanxi Province, National Photoelectric Technology and Functional Materials & Application of Science and Technology International Cooperation Base, Institute of Photonics & Photon-Technology, Northwest University, Xi'an, 710069, China;*

b. *School of Physical Science, University of Science and Technology of China, Hefei, 230026, China;*

---

Author to whom correspondence should be addressed

E-mail: guocf@nwu.edu.cn (Prof. Guo);

Tel & Fax: ±86-29-88302661

## Abstract

A series of green-emitting up-conversion (UC) phosphors $Ba_5Gd_8Zn_4O_{21}$: $Yb^{3+}$, $Ho^{3+}$ were prepared by a modified sol-gel method, and X-ray diffraction (XRD) patterns were measured to characterize the crystal structure. *The obtained* UC samples emit dazzling green light and their spectra *are composed of strong* green emission peaked at 544 nm and negligible red emission peaked at 666 nm with the excitation of 980 nm near-infrared (NIR) *laser diode*, assigned to $^5F_4/^5S_2 \rightarrow {}^5I_8$ and $^5F_5 \rightarrow {}^5I_8$ transitions of $Ho^{3+}$, respectively. The dependence of UC spectra on dopant contents, temperature and pumping power were employed to analysis UC emission *color* stability. The possible UC mechanisms and processes were proposed based on dependence of UC emission intensity on pump power, and the lifetimes of green emission ($^5F_4/^5S_2 \rightarrow {}^5I_8$) were also investigated to better comprehend energy transfer (ET) process. The origin of spectrally pure green-emitting was discussed in detail by analyzing UC and down-conversion (DC) spectra in both visible and NIR region by comparing *that of UC phosphor* $CaIn_2O_4$*:* $Yb^{3+}/Ho^{3+}$ *with high efficient green emitting*. Results suggest that $Ba_5Gd_8Zn_4O_{21}$: $Yb^{3+}$, $Ho^{3+}$ *phosphors* with *intense green emission* and high color purity have potential applications in display and illuminating technology.

**Keywords:** Up-conversion; Phosphor; Energy transfer.

## 1. Introduction

Up-conversion (UC) phosphors could convert low-energy infrared (IR) light with long wavelength to high-energy visible or ultraviolet (UV) light with short wavelength through the *multi-photon absorption process*. Rare earth (RE) ions are generally used as *luminescence centers of* the UC phosphors because of their abundant electronic states, long-lived intermediate meta-stable states and ladder-like arranged energy levels [1]. And *researches* on lanthanide ions doped UC phosphors *have* been exceedingly stimulated by their multiple potential applications in illuminating *technology*, displays, biological imaging, solar cells, laser crystals and optical sensors [*2-8*]. However, the abundant 4*f* electronic states of RE ions generally lead to multicolor emitting with several emission peaks from *f-f* transitions, *and* it is necessary to quantify or purify the emission color in some special applications such as display and illuminating fields [9]. As one of three primary colors, green UC emission can be obtained from rare earth ions $Er^{3+}$ ($^2H_{11/2} \rightarrow {}^4I_{15/2}$/ $^4S_{3/2} \rightarrow {}^4I_{15/2}$), $Pr^{3+}$ ($^1I_6 \rightarrow {}^3H_5/{}^3P_0 \rightarrow {}^3H_5$), $Tb^{3+}$ ($^5D_4 \rightarrow {}^7F_5$), $Nd^{3+}$ ($^2P_{1/2} \rightarrow {}^4I_{13/2}$, $^4G_{7/2} \rightarrow {}^4I_{9/2}$), $Sm^{3+}$ ($^4G_{5/2} \rightarrow {}^6H_{5/2}$) and $Ho^{3+}$ ($^5F_4/{}^5S_2 \rightarrow {}^5I_8$) under the excitation of near-infrared *(NIR)* light [10]. Among these lanthanide ions, $Ho^{3+}$ ion may *exhibit* predominantly green UC emission in *low-phonon* energy hosts, but small absorption cross-section *of* $Ho^{3+}$ *in NIR region* usually leads to low efficiency. As an efficient sensitizer, $Yb^{3+}$ ion could *offer* intense absorption band around 980 nm as well as well-matched excited levels with $Ho^{3+}$ ($^5I_8$), which could *harvest* more pumping photons and subsequently *transfer* them to adjacent activator ions effectively [11].

To obtain spectrally pure up-conversion luminescence (UCL) in $Ho^{3+}$ doped phosphors, several attempts have been made to design high purity of single-band emission UC phosphors [12]. *It is a popular method by incorporating different ions in a single host to selectively populate specific energy levels of RE luminescent centers through energy transfer process.* For example, high red to green ratio can be realized by introducing $Ce^{3+}$ ion into $Yb^{3+}/Ho^{3+}$ system, but it sacrifices the overall UCL intensities *because of concentration quenching effect* [13]. In addition, the color purity of UC emission could also be tuned by adjusting the *phonon* energy of host. Employing appropriate matrixes with low *phonon* energy is a promising way, in which single-band emission as well as high UC efficiency could be achieved by inhibiting *non-radiative decay process*. Up to

now, fluoride-based UC phosphors are considered to be the most efficient UC hosts because of lower phonon energy, such as the hexagonal $\beta$-$NaYF_4$ *which is considered as* the most efficient *host*, yet poor physical and chemical stabilities restrict their further applications [14]. Oxide based host with relatively low *phonon* energy is an ideal selection, which could *offer* both high UCL efficiency as well as stable thermal and chemical properties [15]. Among them, high UCL efficiency of 5.5% as well as perfect spectral color purity was reported in $Yb^{3+}/Ho^{3+}$ doped oxide host $CaIn_2O_4$ [16].

Zincate complex oxide $Ba_5Gd_8Zn_4O_{21}$ offers not only excellent stability but also low phonon energy (472 $cm^{-1}$) which is an ideal UC matrix. Thus, $Yb^{3+}/Ho^{3+}$ co-doped $Ba_5Gd_8Zn_4O_{21}$ UC phosphors were prepared by a sol-gel process, and it could be deduced that the present system could offer *excellent* UC efficiency according to previous investigations [17-18]. The mechanism that affects the UC emission color purity was studied in detail, and the stability of emission color with various dopant contents, temperature and pumping power were also discussed. Moreover, the origin of strong *green emission* intensity and spectral color purity in $Yb^{3+}/Ho^{3+}$ co-doped $Ba_5Gd_8Zn_4O_{21}$ was investigated in a comparable method by using $CaIn_2O_4$: $Yb^{3+}/Ho^{3+}$ phosphor as *a* reference.

## 2. Experimental

### 2.1 Sample Preparation

The $Yb^{3+}$ sensitized $Ho^{3+}$ doped $Ba_5Gd_8Zn_4O_{21}$ (BGZ) phosphors and blank sample were prepared using a modified sol-gel process. Here, $Yb^{3+}$ and $Ho^{3+}$ are expected to enter the sites of $Gd^{3+}$ due to their similar ionic radius and identical valence, and the nominal formula was $Ba_5Gd_{8(1-x-y)}Ho_{8x}Yb_{8y}Zn_4O_{21}$ ($x$ = 0.1-1% and $y$ = 0-10%). *High* purity $Gd_2O_3$, $Yb_2O_3$ and $Ho_2O_3$ (99.99%, Shanghai Yuelong Nonferrous Metals Ltd.), analytical grade (A. R.) $BaCO_3$, ZnO and citric acid were used as raw materials and weighed according to *their* stoichiometric ratio. At the beginning, the required amount of rare earth oxides $Ln_2O_3$ (Ln = Gd, Yb and Ho) were dissolved in $HNO_3$ (A. R.) solution with consecutive heating and stirring. The excessive $HNO_3$ was removed by evaporation, and suitable volume of de-ionized water was added with vigorous stirring to form transparent solution. After that, the calculated quantity of citric acid (molar ratio of citric acid to

total metal ions was 2:1) was introduced into the above solution as chelating agent. Subsequently, $BaCO_3$ *and* ZnO were introduced and stirred for several minutes to obtain transparent aqueous solution. The obtained solution was kept in an oven at 70 ℃ for 24 h to get colorless transparent resin, then further dried at 120 ℃ for 24 h to get brown dried gel. Finally, the grinded dried gel was pre-heated for 5 h at 500 ℃ and then sintered at 1200 ℃ for 3 h to gain the final samples. The reference $CaIn_2O_4$: $Yb^{3+}$/$Ho^{3+}$ phosphors were prepared through a similar process to reference [15].

### 2.2 Measurements and characterization

The powder X-ray diffraction (XRD) data were collected over an angular $2\theta$ range from 20° to 60° using a Rigaku-Dmax 3C diffractometer (Rigaku Corp, Tokyo, Japan) with Cu-$K\alpha$ ($\lambda$ = 1.54056 Å) radiation. Fourier transform infrared spectroscopy (FT-IR) spectra were measured in the range of 400-4000 $cm^{-1}$ on a Bruker Optics EQUINOX55 spectrometer, using pressed KBr tablets. The up/down-conversion photoluminescence (PL) spectra of phosphors at different temperature in the visible and near-infrared region were recorded on an Edinburgh Instruments FLS920 spectrometer equipped with a 450 W Xe lamp and an Oxford OptistatDN2 nitrogen cryogenics temperature controlling system. For the UC luminescence, an external power-controllable 980 nm semiconductor laser were used as excitation source. The measurement of lifetime for $^5F_4/^5S_2 \rightarrow {}^5I_8$ transitions of $Ho^{3+}$ at room temperature (RT) *was* carried out using 980 nm pulsed laser *from* an optical parametric oscillator (OPO) as excitation source, and the signals were analyzed by a Tektronix digital oscilloscope (TDS 3052).

## 3. Results and discussion

### 3.1 Phase purity and structure

XRD was used to identify the crystal structure and phase purity of the powder samples in present experiments, and all obtained samples show similar XRD patterns. Thus, only the XRD patterns of blank BGZ, singly doped BGZ: 0.5%$Ho^{3+}$ and co-doped BGZ: 0.5%$Ho^{3+}$, 5%$Yb^{3+}$ *samples* were presented in Fig.1a as representatives. All the observed diffraction peaks of phosphors coincide well with the standard BGZ data JCPDS No. 51-1686 and no additional diffraction peaks related to raw materials or impurities were detected, indicating the formation of single phase with no impurities. For $Ba_5Gd_8Zn_4O_{21}$, it crystallizes in the tetragonal space group

*I4/m*, in which there are two types of BaO polyhedra: bicapped square prisms ($BaO_{10}$) and irregular polyhedral ($BaO_{10}$). $Zn^{2+}$ ions adopt a fivefold distorted square pyramidal coordination, and the seven-coordinate $Gd^{3+}$ resides in monocapped trigonal prisms. These prisms share edges and form layers stacked along the *c* axis, as shown in Fig.1c [19]. It can be reasonably supposed *that* $Ho^{3+}$ /$Yb^{3+}$ partially substituted the sites of $Gd^{3+}$ due to the similarity of their radii, which releases the restriction on the acceptable doping level. The significantly shift of diffraction peaks from the low towards the higher angles was observed with the increase of *dopant* concentration, and the enlarged peaks (321) were shown in Fig.1b. The calculated cell parameters according to the obtained XRD data are $a = b = 13.947$ Å, $c = 5.723$ Å, $V = 1113.231$ Å$^3$ for BGZ, $a = b =$ 13.901Å, $c = 5.733$ Å, $V = 1105.899$ Å$^3$ for BGZ: $Ho^{3+}$ and $a = b = 13.822$ Å, $c = 5.698$ Å, $V =$ 1093.366 Å$^3$ for BGZ: $Ho^{3+}$, $Yb^{3+}$. Above results *suggest* that the cell parameters gradually decreases with the addition of dopants due to the smaller radii of $Ho^{3+}$ ($R_{Ho} = 0.958$ Å) and $Yb^{3+}$ ($R_{Yb} = 0.925$ Å) than that of $Gd^{3+}$ ($R_{Gd} = 1.00$ Å) for coordination number (CN) = 7, indicating that the $Ho^{3+}$/$Yb^{3+}$ ions efficiently doped into the crystal lattice.

### 3.2 Stability of *UC* emission color

The UC emission spectra of the as synthesized BGZ: $Ho^{3+}$, $Yb^{3+}$ phosphors excited by continuous near-infrared (NIR) 980 nm laser at room temperature were presented in Fig. 2a and b, respectively. Those are composed of intense green emission bands at 544 nm from $^5F_4/^5S_2 \rightarrow {}^5I_8$ transitions and negligible weak red band at 666 nm from $^5F_5 \rightarrow {}^5I_8$ transitions of $Ho^{3+}$. *As well-known*, $Ho^{3+}$ ions are activators and luminescence centers, while the $Yb^{3+}$ ions *are sensitizers* to enhance the UC efficiency. Generally, the concentration of activator and sensitizer greatly influence the UC intensity, thus the optimal composition of phosphors was determined. Fig. 2a shows the UC spectra of BGZ: 0.5%$Ho^{3+}$, *y*$Yb^{3+}$ samples under NIR 980 nm excitation, in which the concentration of activator $Ho^{3+}$ was fixed at 0.5% and contents of sensitizer *varied* from 0 to 10%. It is clearly observed that UC intensity abruptly enhanced with the introduction of sensitizer due to the larger absorption cross-section of $Yb^{3+}$ (~ $10^{-20}$ cm$^2$) than that of $Ho^{3+}$ (~ $10^{-21}$ cm$^2$) at 980 nm, thus the emission spectrum of $Ho^{3+}$ solely doped sample was compressed into a horizontal line in comparison with those of co-doped samples [20]. This result indicates that efficient energy transfer from $Yb^{3+}$ to $Ho^{3+}$ occurred owing to the significant spectra overlap between the emission of $Yb^{3+}$ transition $^2F_{5/2} \rightarrow {}^2F_{7/2}$ and the $^5I_8 \rightarrow {}^5I_6$ absorption band of $Ho^{3+}$.

With the increase of $Yb^{3+}$ concentration, more excitation energy from 980 nm laser diode can be absorbed by $Yb^{3+}$ and more energy can be transferred to $Ho^{3+}$, leading to the increase of UCL intensity. After reaching the maximum at $y$ = 5%, the UCL intensity decreases due to the concentration quenching effect or the energy back transfer (EBT) process from $Ho^{3+}$ to $Yb^{3+}$: $Ho^{3+}$ ($^5F_4/^5S_2$) + $Yb^{3+}$ ($^2F_{7/2}$) → $Ho^{3+}$ ($^5I_6$) + $Yb^{3+}$ ($^2F_{5/2}$) [21]. For the constant $Yb^{3+}$ content ($y$ = 5%) *and variable* $Ho^{3+}$ *content*, similar trend was found and the optimal $Ho^{3+}$ concentration was determined to be about 0.5% according to corresponding *UCL* intensity (Fig. 2b). Where UC intensity first gradually becomes stronger and then decreases as the contents of $Ho^{3+}$ beyond 0.5% because of the concentration quenching effect occurred at high concentration by non-radiative energy loss among the dopants. In comparison, all profiles of UC spectra are similar except relative intensity, and dominated by *an* intense green emission. For the red emission band, the enlarged red band was shown in the inset of Fig. 2b, which *exhibits* a similar variable trend with green bands though it is too weak.

The obtained samples exhibit intense spectrally pure green emissions for naked eyes, and the digital photograph of the sample BGZ: 0.5%$Ho^{3+}$, 5%$Yb^{3+}$ with optimal composition dispersing in ethanol under the excitation of 980 nm NIR light was shown in the inset of Fig. 2c. According to corresponding UC spectra and the digital photo, it could be deduced that the present *phosphors* offer pure green emission. The Commission International del'Eclairage (CIE) chromaticity coordinates of all samples were calculated and insert in the Fig.2a, it is found that the CIE chromaticity coordinates of all co-doped samples BGZ: $Ho^{3+}$/$Yb^{3+}$ are close to (0.295, 0.696) and hardly changed, indicating that the emission color of present phosphors is independent of dopant contents. The CIE chromaticity diagram clearly shows the location of emission color in the range of green region, which were presented in Fig. 2c.

The stability of emission color seriously affects the performance of the device in the process of application. High pumping power is usually used to enhance the efficiency of UC phosphor, which would lead to the increasing of working temperature of phosphor. Therefore, the power and temperature-dependent UC emission of sample BGZ: 0.5%$Ho^{3+}$, 5%$Yb^{3+}$ were representatively investigated as a function of pumping power and temperature, *as* shown in Fig. 3. Figure 3a shows normalized UC spectra under the excitation of 980 nm NIR laser (pumping power 20 mW) with various temperatures ranging from room temperature to 490 K, in which no remarkable change

was found. The UC spectra are still dominated by the green emission from transition $^5F_4/^5S_2 \rightarrow {}^5I_8$, and the red *emissions* are not significantly enhanced. Comparing with Fig.3a, similar status was also observed in the normalized UC spectra (Fig. 3b) with the increasing of pumping power from 710 to 1838 mW. The corresponding integrated intensity ratio of red to green is close to a constand 0.070 (as shown in Fig.3a) and is hardly influenced by temperature and pumping power. Moreover, the CIE coordinates were also calculated according to their emission spectra and displayed in the insert of Fig.3b, those are close to a constant (0.295, 0.697) for the different temperature and the various pumping power in our experiments. Above phenomena imply that the present spectrally pure green emission in BGZ: $Ho^{3+}$, $Yb^{3+}$ phosphor offer excellent color stability which could isolate from the impact of temperature of external environment and pumping power.

### 3.3 *Mechanism of Spectrally pure green UC emission*

To better understand the observed phenomenon, the UC mechanisms of green and red emission were studied according to the dependence of the UCL intensity $I_{f\text{-}f}$ on the pumping power of 980 nm laser diode $P_{980}$, which generally abides the following equation: $I \propto P^n$ [22]. Here, the *value* of *n* denotes the number of the NIR photons absorbed per up-converted photon emitted, which equals to the slope of the straight line by fitting the plot of log *I versus* log *P*. To determine the number of NIR photons required for the UC process, the double logarithmic plots of integrated green (525-575 nm) and red (630-680 nm) intensity of BGZ: 0.5%$Ho^{3+}$, 5%$Yb^{3+}$ phosphor as a function of pumping power were plotted in Fig. 4a. It is found that the obtained slopes for red and green emission are 1.64 and 2.36, suggesting that the red emission is two-photon absorption process whereas the green emission maybe a mixing process of two-photon and three-photon.

According to above results, the possible population processes in BGZ: $Ho^{3+}$, $Yb^{3+}$ samples were schematically given in the energy level diagrams of $Ho^{3+}$ and $Yb^{3+}$ with feasible transitions, as demonstrated in Fig. 4b. Under the excitation of 980 nm, the $^2F_{2/7}$ + *a photon (980 nm)* $\rightarrow {}^2F_{2/5}$ transition of $Yb^{3+}$ occurs by absorbing an infrared photon. For the green emission from $^5F_4/^5S_2 \rightarrow {}^5I_8$ transition, the excited levels $^5F_4/^5S_2$ could be populated via a two-photon or three-photon process. The former process is achieved *via* ET process: $Yb^{3+}$ ($^2F_{5/2}$) + $Ho^{3+}$ ($^5I_6$) $\rightarrow$ $Yb^{3+}$ ($^2F_{7/2}$) + $Ho^{3+}$ ($^5F_4/^5S_2$) or excitation state absorption (ESA): $Ho^{3+}$ ($^5I_6$) + a photon (980 nm) $\rightarrow$ $Ho^{3+}$ ($^5F_4/^5S_2$). The intermediary level $^5I_6$ of $Ho^{3+}$ is populated by ground state absorption (GSA): $Ho^{3+}$ ($^5I_8$) + a 980 nm photon $\rightarrow$ $Ho^{3+}$ ($^5I_6$) or energy transfer (ET) from $Yb^{3+}$ to $Ho^{3+}$: $Yb^{3+}$ ($^2F_{5/2}$) +

$Ho^{3+}$ ($^5I_8$) → $Yb^{3+}$ ($^2F_{7/2}$) + $Ho^{3+}$ ($^5I_6$). Compared with GSA process, ET process is the predominant owing to lager absorption cross section *at 980 nm* of $Yb^{3+}$ than that of $Ho^{3+}$. As for the three-photon process, the $^5F_4/^5S_2$ level is populated by non-radiative (NR) transition from $^5F_2$ level. The population of metastable state $^5I_4$ is a result of cross relaxation (CR) process: $Ho^{3+}$ ($^5F_4/^5S_2$) + $Ho^{3+}$ ($^5I_8$) → $Ho^{3+}$ ($^5I_4$) + $Ho^{3+}$ ($^5I_7$), and could be excited to upper level $^5F_2$ *via* ET process: $Yb^{3+}$ ($^2F_{5/2}$) + $Ho^{3+}$ ($^5I_4$) → $Yb^{3+}$ ($^2F_{7/2}$) + $Ho^{3+}$ ($^5F_2$). In above mentioned two processes, two-photon process plays a dominant role due to low probability of CR. Finally, the population at $^5F_4/^5S_2$ levels decays radiatively to ground state with green emission at 544 nm. For the 666 nm red emission from $^5F_5$ → $^5I_8$ transition, the population at $^5F_5$ level could be achieved through two possible processes. One is exciting population at long-lived $^5I_7$ level to upper state $^5F_5$ level by ET process: $Yb^{3+}$ ($^2F_{5/2}$) + $Ho^{3+}$ ($^5I_7$) → $Yb^{3+}$ ($^2F_{7/2}$) + $Ho^{3+}$ ($^5F_5$) after NR transition of $^5I_6$ → $^5I_7$. In addition, the three-photon process of green emission is also in favor of red *emission* due to the above mentioned CR process. The other *possible process* is NR transition from $^5F_4/^5S_2$ to $^5F_5$. Thus, radiative relaxation from $^5F_5$ level to ground state generates red emission at around 666 nm. Additionally, over high $Yb^{3+}$ contents would lead to predominance of EBT process from $Ho^{3+}$ to $Yb^{3+}$: $Ho^{3+}$ ($^5F_4/^5S_2$) + $Yb^{3+}$ ($^2F_{7/2}$) → $Ho^{3+}$ ($^5I_6$) + $Yb^{3+}$ ($^2F_{5/2}$).

Above analysis proves that the red emission strongly depends on the NR transition probability, and the phonon-assisted non-radiative transition probability in materials is principally influenced by the *phonon* energy of the matrix. The non-radiative decay rate (*W*) could be mathematically written as: [23]

$$W(T) = W(0)[\frac{\exp(h\nu / kT)}{\exp(h\nu / kT) - 1}]^{\Delta E / h\nu} \quad (1)$$

where *T* is absolute temperature; *W(T)* and *W(0)* is the non-radiative decay rate at temperature T and 0 K, respectively; *k* is Boltzmann constant, *ΔE* denotes the energy gap between two levels and *hν* is the *phonon* energy of the host matrix.

Fig 5 displayed the UCL spectrum of BGZ: 0.5%$Ho^{3+}$, 5%$Yb^{3+}$ phosphor at 80 K, in which the red emission ($^5F_5$ → $^5I_8$) completely *disappears* and the green emissions from $^5F_4$ and $^5S_2$ → $^5I_8$ are divided. These phenomena are caused by low non-radiative transition rate at 80 K in samples, which is coincided with equation (1). As the energy gap between two levels is 4 ~ 5 times larger than that of the *phonon* energy of host matrix on the basis of energy gap law, multi-photon

relaxation is predominate and non-radiative hardly happen [24]. The FT-IR spectrum of blank BGZ was carried out to determine the *phonon* energy of host, as shown in the inset of Fig. 5. The strongest *phonon* cut-off energy band at 472 $cm^{-1}$ could be assigned to the stretching vibrations of Zn-O, which demonstrates that the *phonon* energy of the BGZ is approximately 472 $cm^{-1}$. The energy gap between $^5I_6$ and $^5I_7$ states (3450 $cm^{-1}$) and that of $^5F_4/^5S_2$ and $^5F_5$ levels (3000 $cm^{-1}$) of $Ho^{3+}$ is about 6 ~ 7 times larger than that of the host *phonon* energy, which means seven or more phonons are involved to bridge above energy gap. Result indicates that the probability of non-radiative transition $^5I_6 \rightarrow {}^5I_7$ and $^5F_4/^5S_2 \rightarrow {}^5F_5$ is negligible and high population at $^5F_4/^5S_2$ energy levels can be achieved, leading to a extremely weak red emission and spectrally pure green-emitting (as presented in Fig. 2a and b).

According to above investgation, it can be deduced that the efficient ET from $Yb^{3+}$ to $Ho^{3+}$ ions contributes a *lots* to enhance UC intensities. To further prove the occurance of ET process, the normalized temporal curves of the green emission from $^5F_4/^5S_2 \rightarrow {}^5I_8$ transition in BGZ: 0.5%$Ho^{3+}$, *y*$Yb^{3+}$ (*y* = 5, 10%) were measured in Fig. 6 with 980 nm pulsed laser excitation. The transient of intensity *exhibits* an obvious distinct prolonged rise part at the end of the excitation, which proves the presence of the ET process [25]. With increasing $Yb^{3+}$ content (*y*) from 5 to 10%, the ionic distance *becomes* closer and more efficient ET process occurs, leading to shorter rising time in the temporal curves, as shown in the inset of Fig. 4. It should be noted that the decay curve of $Ho^{3+}$ single doped BGZ cannot be accurately monitored because of its weak emission intensity.

The effective lifetime of emitting level could be calculated using following equation (2): [26]

$$\tau = \frac{\int_0^\infty I(t)tdt}{\int_0^\infty I(t)dt} \tag{2}$$

where *I*(*t*) denotes the UCL intensity at time *t*. The temporal profile can be fitted with a quadratic exponential function and the average lifetime can be defined as: [27]

$$\bar{\tau} = \frac{A_1 t_1^{\ 2} + A_2 t_2^{\ 2}}{A_1 t_1 + A_2 t_2} \tag{3}$$

where *A* and *t* represent the amplitude and lifetime corresponding to the level depopulation channel, respectively. As listed in Fig. 6, the obtained lifetime of $^5S_2/^5F_4$ states decreases from 161.26 to 59.23 μs as increasing $Yb^{3+}$ content from 5 to 10%. It can be explained by the

convenient EBT process: $Ho^{3+}$ ($^5F_4/^5S_2$) + $Yb^{3+}$ ($^2F_{7/2}$) → $Ho^{3+}$ ($^5I_6$) + $Yb^{3+}$ ($^2F_{5/2}$), and high concentration of $Yb^{3+}$ accelerates the depopulation of $^5S_2/^5F_4$ level and leads to the reduction of lifetime, which is coincided with the variation tendency of green emission intensity shown in Fig. 2b.

### 3.4 Comparison of $Yb^{3+}/Ho^{3+}$ co-doped BGZ and $CaIn_2O_4$

In order to *further* evaluate the green luminescence performance of $Yb^{3+}/Ho^{3+}$ co-doped BGZ phosphor, high-efficiency $CaIn_2O_4$: $Yb^{3+}/Ho^{3+}$ green upconversion phosphor with the maximum UCL efficiency 5.5% (pumping power 1.5 W) *was* employed as a reference [16]. Figure 7 depicted UC spectra of sample with optimal composition BGZ: 0.5%$Ho^{3+}$, 5%$Yb^{3+}$ and $CaIn_2O_4$: 10%$Yb^{3+}$, 0.5%$Ho^{3+}$ using a compariable method, which were measured in the same condition. It clearly observed that the UC spectra of $Ho^{3+}$-$Yb^{3+}$ doped BGZ and $CaIn_2O_4$ two samples are *composed* of dominant green emission ($^5F_4/^5S_2$ → $^5I_8$) and weak red emission ($^5F_5$ → $^5I_8$). Moreover, their red emission intensity is similar but the green emission in BGZ is stronger than that of in $CaIn_2O_4$, and the integrated intensity ratio of green emission (525-575 nm) to red (63 -680 nm) is 19.2 and 18.4 in BGZ and $CaIn_2O_4$ (bar graph in the inset of Fig. 7), respectively. *Results suggest* that the green color purity of BGZ: 0.5%$Ho^{3+}$, 5%$Yb^{3+}$ is higher than those of $CaIn_2O_4$: 10%$Yb^{3+}$, 0.5%$Ho^{3+}$.

To comprehend the origin of *extremely* intense green UCL luminescence, down-conversion (DC) emission spectra of BGZ: 0.5%$Ho^{3+}$, 5%$Yb^{3+}$ and $CaIn_2O_4$: 0.5%$Ho^{3+}$, 10%$Yb^{3+}$ phosphor were measured *under the excitation of 490 nm light* and shown in Fig. 8. Seen from Fig. 8a, it is found that the intensity of green emission in BGZ is larger than that in $CaIn_2O_4$, whereas the *red emission intensities of two phosphors* are very weak and close due to the similar probability of non-radiative (NR) transition in two hosts resulting from their close low phonon energy of BGZ (472 $cm^{-1}$) and $CaIn_2O_4$ (473 $cm^{-1}$). The inset of Fig.8a shows the energy level diagram and possible transition pathways. Here, the incident 490 nm radiation excites an $Ho^{3+}$ ion from its $^5I_8$ ground state to upper excited level $^5F_2$ and then arrives at $^5F_4/^5S_2$ levels by NR1 process ($^5F_2$ → $^5F_4/^5S_2$) transition. Four transition processes are related to $^5F_4/^5S_2$ levels: green radiative transition emission ($^5F_4/^5S_2$ → $^5I_8$), NR2 process ($^5F_4/^5S_2$ → $^5F_5$), CR process ($^5F_4/^5S_2$ + $^5I_8$ → $^5I_4$ + $^5I_7$) and EBT process $Ho^{3+}$ ($^5F_4/^5S_2$) + $Yb^{3+}$ ($^2F_{7/2}$) → $Ho^{3+}$ ($^5I_6$) + $Yb^{3+}$ ($^2F_{5/2}$). It is generally accepted that the probability of CR process greatly depends on the distance of rare earth ions [28]. Considering

that $Ho^{3+}$ content (0.5%) in two hosts is low enough, the probability of CR process is so little that can be ignored. Thus it can be conclude that EBT process significantly influences the green emission intensity. For near-infrared (NIR) DC spectra shown in Fig. 8a, it is observed that NIR emission ($^5I_6 \rightarrow {}^5I_8$) peaked at 1191 nm *in* $Yb^{3+}/Ho^{3+}$ doped $CaIn_2O_4$ *is* stronger than that of BGZ phosphor, which hints that more efficient EBT process occurs in $CaIn_2O_4$, leading to stronger NIR luminescence and weaker green emission. It is well-known that it is a competition process for UC and DC, which plays a vital role in determining UCL intensity. Fig. 8b showed the NIR emission spectra of BGZ: 0.5%$Ho^{3+}$, 5%$Yb^{3+}$ and $CaIn_2O_4$: 0.5%$Ho^{3+}$, 10%$Yb^{3+}$ phosphor under 980 nm laser excitation. Comparing with BGZ phosphor, it is found that $CaIn_2O_4$ phosphor emits stronger 1191 nm NIR emission, which indcitates that the probability of DC process is higher in $CaIn_2O_4$. Namely, BGZ phosphor achieves more efficient UC process than $CaIn_2O_4$ phosphor because of the confrontational relationship between UC and DC process, resulting more intense green UC emission. Therefore, low probability of EBT and NR process as well as efficient UC process against DC process may attribute to the high green UCL intensity and color purity in $Yb^{3+}/Ho^{3+}$ co-doped BGZ phosphor.

## 4. Conclusion

$Ho^{3+}/Yb^{3+}$ co-doped $Ba_5Gd_8Zn_4O_{21}$ (BGZ) up-conversion (UC) phosphors with excellent green emission color purity were synthesized by a sol-gel method, and the optimal composition is BGZ: 0.5%$Ho^{3+}$, 5%$Yb^{3+}$. Their UC spectra are composed of intense green emission (544 nm) from $^5F_4/^5S_2 \rightarrow {}^5I_8$ transition and negligible red emission (666 nm) from $^5F_5 \rightarrow {}^5I_8$ transitions of $Ho^{3+}$ under the excitation of 980 nm light. The stability of color purity is hardly influenced by dopant contents, temperature and pumping power. The UC mechanism and possible processes, along with decay curves of $^5F_4/^5S_2 \rightarrow {}^5I_8$ emission were investigated, in which energy transfer *process* plays a predominant role. Low *phonon* energy of BGZ (472 $cm^{-1}$) is responsible to the weak red UC emission. In addition, high green intensity is originated from low probability of EBT and NR process as well as efficient UC process, which *were* investigated by a comparable method using $CaIn_2O_4$: 10%$Yb^{3+}$, 0.5%$Ho^{3+}$ *phosphor* with the maximum UC efficiency 5.5% as a reference. Results indicate that the present $Yb^{3+}$/ $Ho^{3+}$ co-doped $Ba_5Gd_8Zn_4O_{21}$ phosphors offer

perfect green UC emission and color stability *and could be consider as potential candidates for display and illuminating technology.*

## 5. Acknowledgement

This work was supported by the high-level talent project of Northwest University, National Natural Science Foundation of China (No. 11274251), Research Fund for the Doctoral Program of Higher Education of China (RFDP) (No.20136101110017), Technology Foundation for Selected Overseas Chinese Scholar, Ministry of Personnel of China (excellent), Natural Science Foundation of Shaanxi Province (No.2014JM1004) and Foundation of Key Laboratory of Photoelectric Technology in Shaanxi Province (12JS094).

# References

[1] X. J. Xie and X. G. Liu, *Nat Mater*, 2012, **11**, 842-843

[2] J. Feenstra, I. F. Six, M. A. H. Asselbergs, R. H. van Leest, J. de Wild, A. Meijerink, R. E. I. Schropp, A. E. Rowanb and J. J. Schermera, *Phys. Chem. Chem. Phys*., 2015, **17**, 11234-11243.

[3] S. Mehrabani and A. M. Armani, *Opt. Lett.*, 2013, **38**, 4346-4349.

[4] Y. F. Wang, G. Y. Liu, L. D. Sun, J. W. Xiao, J. C. Zhou and C. H. Yan, *ACS nano*., 2013, **7**, 7200-7206.

[5] B. Dong, B. S. Cao, Y. Y. He, Z. Liu, Z. P. Li and Z. Q. Feng, *Adv. Mater.*, 2012, **24**, 1987-1993.

[6] S. S. Lucky, N. M. Idris, Z. Q. Li, K. Huang, K. C. Soo and Y. Zhang, *ACS nano*., 2015, **9**, 191-205.

[7] E. Downing, L. Hesselink, J. Ralston and R. Macfarlane, *Science*, 1996. **273**, 1185-1189.

[8] J. H. Zhang, Z. D. Hao, J. Li, X. Zhang, Y. S. Luo and G. H. Pan, *Light-Sci. Appl*., 2015, **4**, e239.

[9] R. R. Deng, F. Qin, R. F. Chen, W. Huang, M. H. Hong and X. G. Liu, *Nature nanotechnol*, 2015, **10**, 237-242.

[10] X. M. Li, F. Zhang and D. Y Zhao, *Chem. Soc. Rev.*, 2014, **44**, 1346-1378.

[11] N. M. Sangeetha and F. C. J. M. Van Veggel, *J. Phys. Chem. C*, 2009, **113**, 14702-14707.

[12] J. Wang, F. Wang, C. Wang, Z. Liu and X. G. Liu, *Angew. Chem.*, 2011, **50**, 10369-10372

[13] E. M. Chan, G. Han, J. D. Goldberg, D. J. Gargas, A. D. Ostrowski, P. J. Schuck, B. E. Cohen and D. J. Milliron, *Nano lett.*, 2012, **12**, 3839-3845.

[14] R. H. Page, K. I. Schaffers, P. A. Waide, J. B. Tassano, S. A. Payne and W. F. Krupke, *J. Opt. Soc. Am. B*, 1998, **15**, 996-1008.

[15] R. Kapoor, C. S. Friend, A. Biswas and P. N. Prasad, *Opt. Lett.*, 2000, **25**, 338-340.

[16] T. Li, C. F. Guo, Y. M. Yang, L. Li and N. Zhang, *Acta Mater.*, 2013, **61**, 7481-7487.

[17] I. Etchart, A. Huignard, M. Bérard, M. N. Nordin, I. Hernández, R. J. Curry, W. P. Gillin, and A. K. Cheetham, *J. Mater. Chem*., 2010, **20**, 3989–3994.

[18] B. N. Tian, B. J. Chen, Y. Tian, X. P. Li, J. S. Zhang, J. S. Sun, H. Y. Zhong, L. H. Cheng, S. B. Fu, H. Zhong, Y. Z. Wang, X. Q. Zhang, H. P. Xia and R. N. Hua, *J. Mater. Chem. C*, 2013, **1**, 2338–2344.

[19] W. W. Ng, J. A. Kaduk and J. Dillingham, *Powder Diffr.*, 2001, **16**, 131-143.

[20] G. X. Chen, Q. Y. Zhang, G. F. Yang and Z. H. Jiang, *J Fluoresc*, 2007, **7**, 301-307.

[21] F. M. Li, L. Li, C. F. Guo, T. Li, H. M. Noh and J. H. Jeong, *Ceram Int.*, 2014, **40**, 7363-7366.

[22] M. Pollnau, D. R. Gamelin, S. R. Lüthi, H. U. Güdel, and M. P. Hehlen, *Phys. Rev. B*, 2000, **61**, 3337–3346.

[23] G. Y. Chen, H. C. Liu, H. J. Liang, G. Somesfalean and Z. G. Zhang, *J. Phys. Chem. C*, 2008, **112**,

12030-12036.

[24] J. H. Chung, S. Y. Lee, K. B. Shim and J. H. Ryu, *Appl. Phys. Express*, 2012, 5, 052602.

[25] T. Li, C. F. Guo and L. Li, *Opt. Express*, 2013, **21**, 18281–18289.

[26] H. Jing, C. F. Guo, G. G. Zhang, X. Y. Su, Z. Yang and J. H. Jeong, *J. Mater. Chem*., 2012, **22**, 13612–13618.

[27] T. Fujii, K. Kodaira, O. Kawauchi, N. Tanaka, H. Yamashita and M. Anpo, *J. Phys. Chem. B*, 1997, **101**, 10631–10637.

[28] D. K. Xu, C. F. Liu, J. W. Yan, S. H. Yang and Y. L. Zhang, *J. Phys. Chem. C*, 2015, **119**, 6852-6860.

## Figure captions

**Fig. 1** (a) XRD patterns of prepared samples and the standard profile of BGZ, (b) the corresponding enlarged (321) peaks and (c) projection of the BGZ structure.

**Fig. 2** UCL spectra of BGZ: $x$Ho$^{3+}$, $y$Yb$^{3+}$: (a) $y$ = 0 ~ 10%, $x$ = 0.5% ; (b) $x$ = 0.1 ~ 1%, $y$ = 5%; with corresponding CIE color coordinates insets table; and (c) CIE diagram and UCL photograph of BGZ: 0.5%Ho$^{3+}$, 5%Yb$^{3+}$ phosphor dispersed in ethanol under 980nm excitation.

**Fig. 3** (a) Normalized thermal evolution visible UCL spectra and (b) pump power dependent visible UCL spectra of BGZ: 0.5%Ho$^{3+}$, 5%Yb$^{3+}$ phosphor under 980 nm excitation. Insets show the corresponding red to green ratio and CIE color coordinates.

**Fig. 4** (a) Dependence of visible intensity upon the excitation power in BGZ: 0.5%Ho$^{3+}$, 5%Yb$^{3+}$ phosphor; (b) schematic energy level diagram of Yb$^{3+}$ and Ho$^{3+}$ ions along with the proposed UC mechanisms under 980 nm excitation.

**Fig. 5** UCL spectrum of BGZ: 0.5%Ho$^{3+}$, 5%Yb$^{3+}$ phosphor at 80 K with excitation of 980 nm. The inset shows the FT-IR spectrum of blank BGZ.

**Fig. 6** Luminescence decay curves of 544 nm green emission ($^5F_4/^5S_2 \rightarrow {}^5I_8$) in BGZ: 0.5%Ho$^{3+}$, $y$ Yb$^{3+}$ ($y$ = 5, 10%). Inset shows the enlarged curve of initial ascent stage.

**Fig. 7** Vsible UCL spectra of Yb$^{3+}$/Ho$^{3+}$ co-doped BGZ and $CaIn_2O_4$ phosphor under 980 nm exiciation. Inset shows the corresponding intregated instensity of green and red region and G/R ratio.

**Fig. 8** (a) Visible and near-infared down-conversion emission spectra ($\lambda_{ex}$ = 490nm) and (b) Near-infared emission spectra under the excitation of 980 nm for Yb$^{3+}$/Ho$^{3+}$ co-doped BGZ and $CaIn_2O_4$ phosphor. Inset shows simplified energy diagram.

## Figures

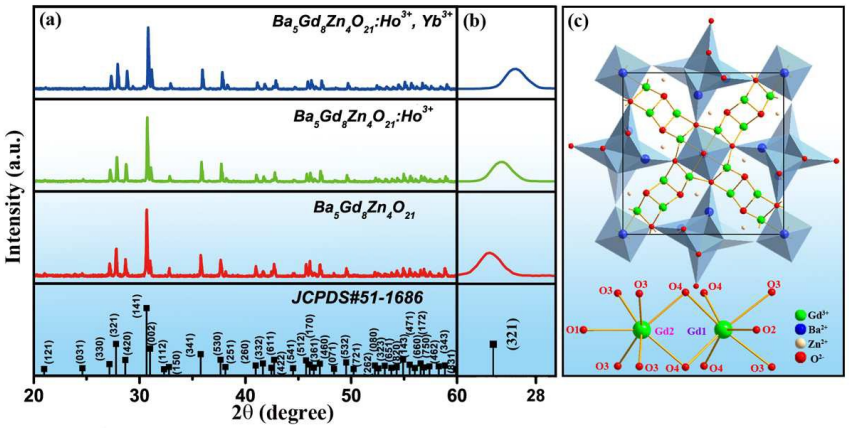


Fig. 1 (a) XRD patterns of prepared samples and the standard profile of BGZ, (b) the corresponding enlarged (321) peaks and (c) projection of the BGZ structure.

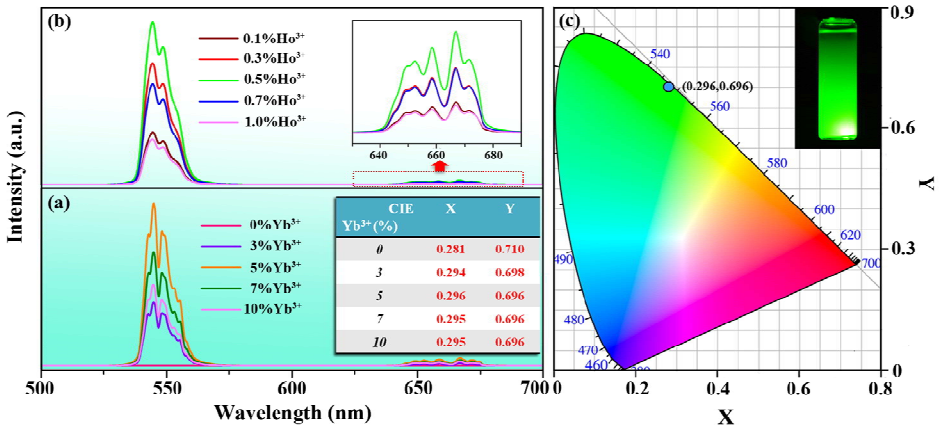


Fig. 2 UCL spectra of BGZ: $x$ $Ho^{3+}$, $y$ $Yb^{3+}$: (a) $y$ = 0 ~ 10%, $x$ = 0.5% ; (b) $x$ = 0.1 ~ 1%, $y$ = 5%; with corresponding CIE color coordinates insets table; and (c) CIE diagram and UCL photograph of BGZ: 0.5%$Ho^{3+}$, 5%$Yb^{3+}$ phosphor dispersed in ethanol under 980nm excitation.

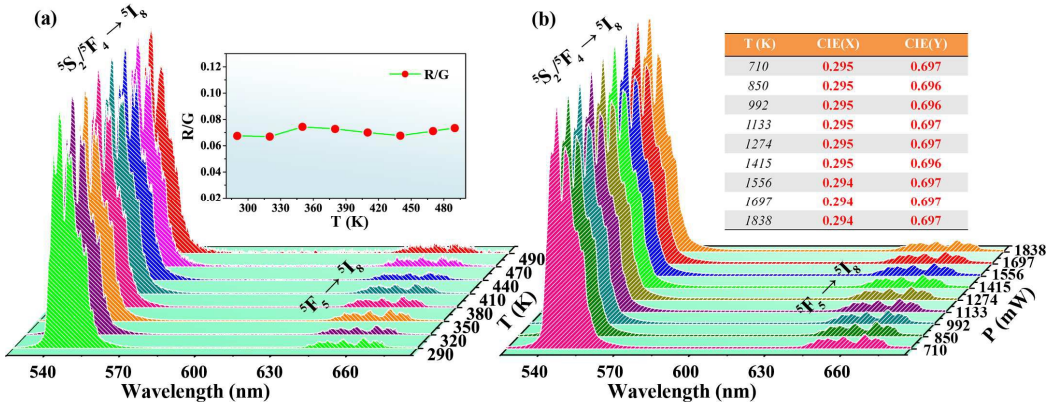


Fig. 3 (a) Normalized thermal evolution visible UCL spectra and (b) pump power dependent visible UCL spectra of BGZ: 0.5%$Ho^{3+}$, 5%$Yb^{3+}$ phosphor under 980 nm excitation. Insets show the corresponding red to green ratio and CIE color coordinates.

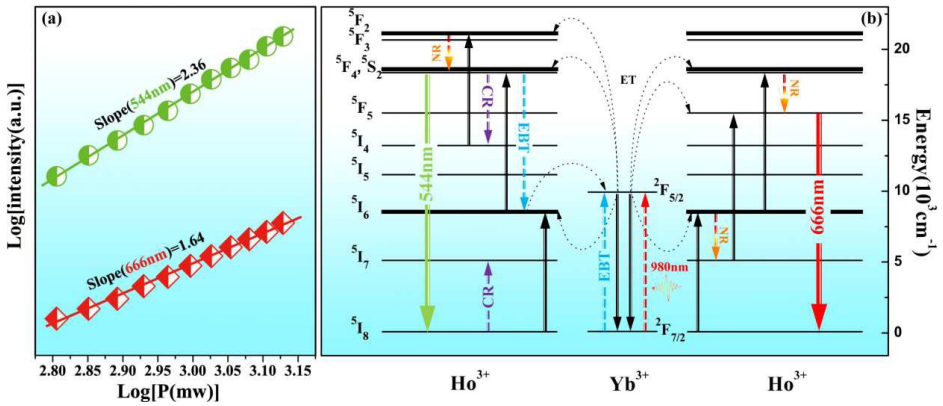


Fig. 4 (a) Dependence of visible intensity upon the excitation power in BGZ: 0.5%$Ho^{3+}$, 5%$Yb^{3+}$ phosphor; (b) schematic energy level diagram of $Yb^{3+}$ and $Ho^{3+}$ ions along with the proposed UC mechanisms under 980 nm excitation.

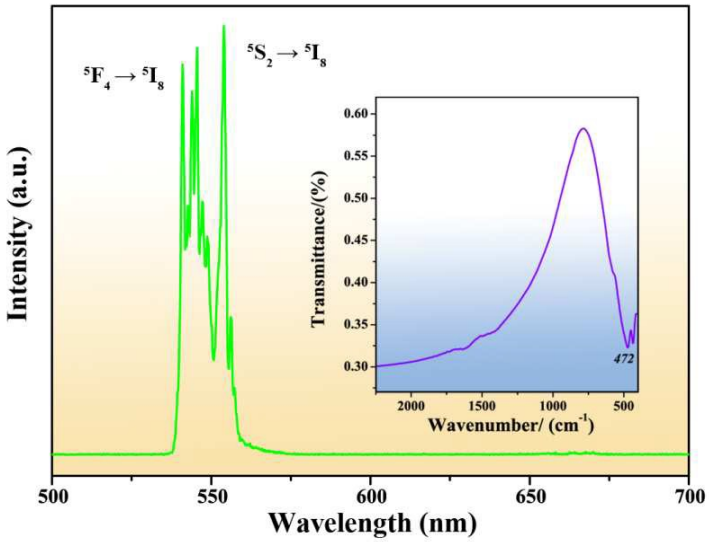


Fig. 5 UCL spectrum of BGZ: 0.5%$Ho^{3+}$, 5%$Yb^{3+}$ phosphor at 80K with excitation of 980 nm. The inset shows the FT-IR spectrum of blank BGZ.

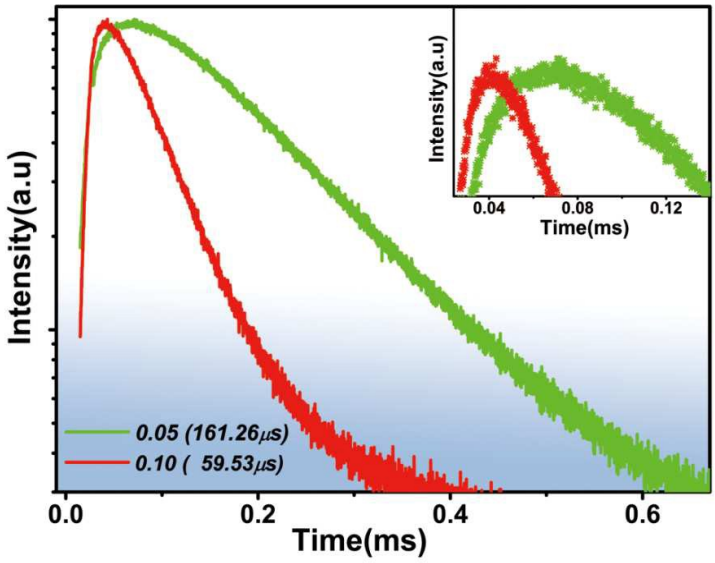


Fig. 6 Luminescence decay curves of 544 nm green emission ($^5F_4/^5S_2 \rightarrow {}^5I_8$) in BGZ: 0.5%$Ho^{3+}$, *y* $Yb^{3+}$ (*y* = 5, 10%). Inset shows the enlarged curve of initial ascent stage.

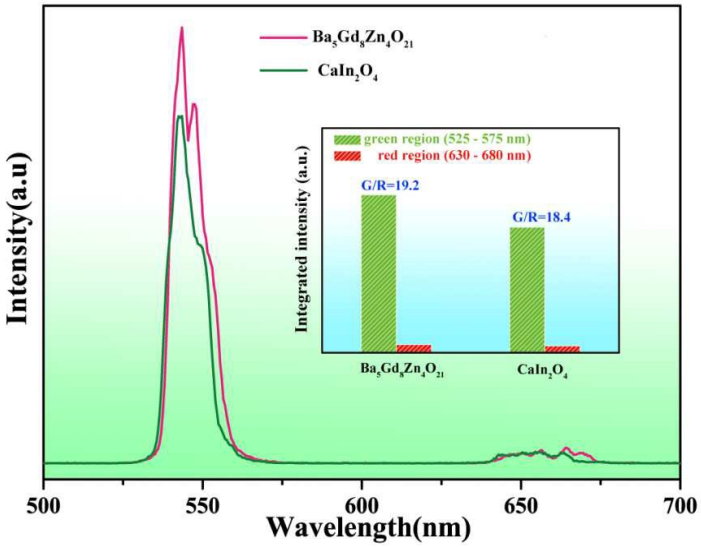


Fig. 7 Vsible UCL spectra of $Yb^{3+}/Ho^{3+}$ co-doped BGZ and $CaIn_2O_4$ phosphor under 980 nm exiciation.Inset shows the corresponding intregated instensity of green and red region and G/R ratio.

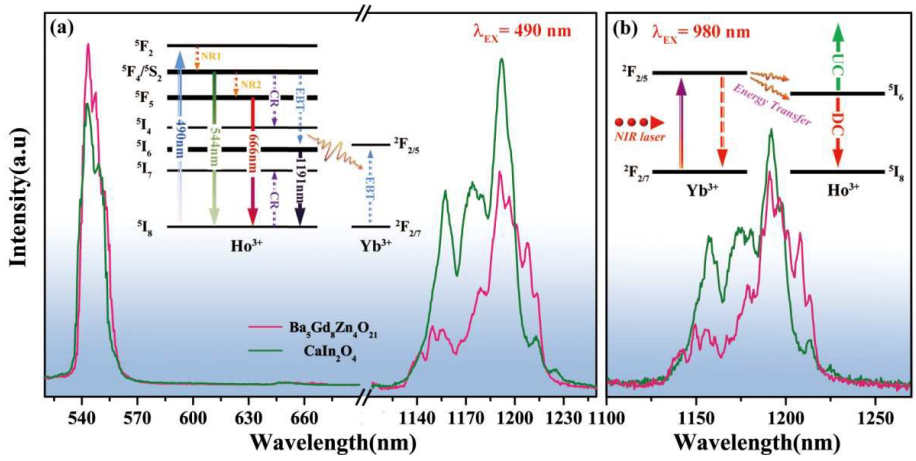


Fig. 8 (a) Visible and near-infared down-conversion emission spectra ($\lambda_{ex}$=490nm) and (b) Near-infared emission spectra under the excitation of 980 nm for $Yb^{3+}/Ho^{3+}$ co-doped BGZ and $CaIn_2O_4$ phosphor. Inset shows simplified energy diagram.

# Graphic abstract

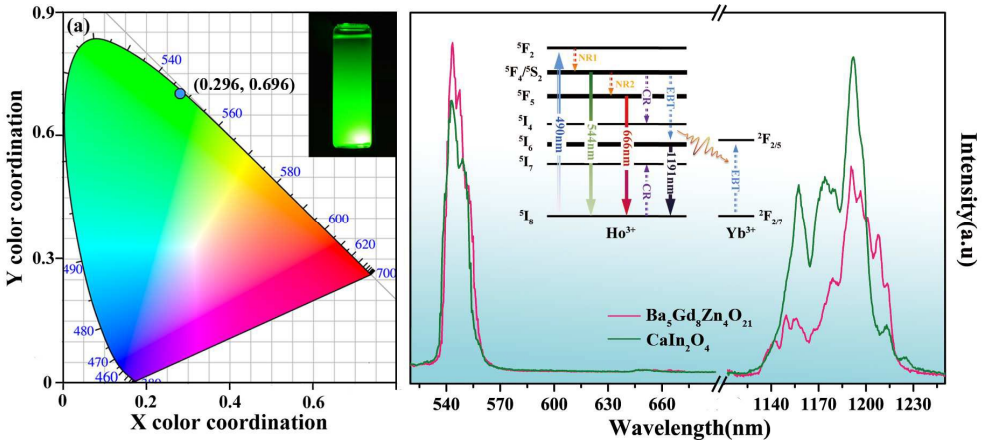


Figure. CIE diagram and spectrally pure green emission mechanism of $Ba_5Gd_8Zn_4O_{21}$: $Yb^{3+}$, $Ho^{3+}$ phosphors.

## Textual abstract for the contents pages

Intense green emitting UC phosphor isolates from the impact of dopant content, temperature and pumping power.